Direct Imaging of Habitable Exoplanets with ELTs

Olivier Guyon[1,2a]

[1] Subaru Telescope
[2] University of Arizona

Abstract. The unprecedented angular resolution soon to be offered by extremely large telescopes (ELTs), together with recently developed high contrast imaging techniques (coronagraphy and wavefront control), can enable direct imaging and spectroscopic characterization of potentially habitable planets around nearby M-type stars. While the habitable zone of M stars is challenging to resolve, the planet to star contrast and the apparent brightness of the planet are highly favorable, thus providing the only opportunity for direct imaging and spectroscopic characterization of habitable planets from the ground. The key to imaging and characterizing such planets lies in the ability to perform high contrast imaging (approximately 1e-5 raw contrast) at 1 to 2 λ/D with high photometric efficiency. We demonstrate that technical solutions to this challenge exist: a full throughput coronagraph concept offering sub-λ/D inner working angle at high contrast on segmented aperture is shown, and schemes to achieve the necessary level of pointing and low order wavefront error control are presented. Demonstrations of these key techniques are ongoing in laboratories and on ground-based telescopes, already yielding encouraging results. We conclude that a highly specialized, but relatively simple, high contrast imaging system can be build for ELTs within this decade, and that it would likely provide the first opportunity to acquire high quality spectra of habitable planets, before space-based telescope can provide similar capabilities for brighter F-G-K type stars.

1 Outline

In Section 2, the expected first-order observational characteristics (planet contrast, separation and apparent luminosity; star brightness) of rocky planets in the habitable zones of nearby stars are established. Using these parameters, section 3 shows that rocky planets around M-type stars can be observed with ELTs in reflected light provided that (1) a coronagraph operating with a 1 λ/D inner working angle can be used and (2) wavefront sensing can be performed efficiently on low-order aberrations. These two requirements are then discussed in more detail in sections 4 (coronagraphy) and 5 (wavefront control and calibration). System architecture and technological choices are discussed in section 6.

2 Rocky Planets in Habitable Zones of Nearby Stars

2.1 Input catalogs

In this section, we evaluate the expected photometric properties of rocky planets in the habitable zones of nearby stars. For simplicity, we consider planets with an albedo equal to 0.3, independent of wavelength, and with diameters exactly twice the Earth diameter. Planets are placed on circular orbits with semi-major axis equal to one astronomical unit multiplied by the square root of the star bolometric luminosity (relative to the Sun). The planet thus receives from its star the same total flux per unit of area as Earth. Observations of the planets are assumed to be at maximum elongation. Three catalogs are used to construct the input target catalog:

- The Gliese Catalog of Nearby Stars 3rd edition (CNS3) [1] containing all stars known to be within 25 parsecs of the Sun as of 1991. This catalog is the primary source of targets for this work, and contains the position the spectral type, apparent magnitude (V band), colors (B-V, R-I) and parallax for each target.
- Near-IR photometry is obtained from the 2MASS point source catalog [2,3].

[a] guyon@naoj.org

– The northern 8-parsec sample [4] contains bolometric luminosities and colors (B-V, V-R, V-I) is used to establish empirical photometric relationships that can be applied to the full Gliese catalog

2.2 Star bolometric luminosity, planet angular separation and contrast

The bolometric correction, required to derive the bolometric luminosity of each star of the sample from its absolute magnitude in V band, is derived from the 8-pc sample, which does include, for each star, both the absolute V magnitude and the bolometric magnitude. Since the bolometric is mostly a function of stellar temperature, the bolometric correction is fitted as a function of B-V color for the 8-pc sample.

The bolometric luminosity (referenced to the Sun) for each star is then derived from the absolute magnitude M_V and the bolometric correction BC:

$$L_{bol} = 2.51188643^{-(M_V - 4.83)+(BC-BC_{Sun})} \quad (1)$$

with $BC_{Sun} = -0.076$.

The planet is then placed $\sqrt{L_{bol}}$ AU from the star, and its angular separation is computed using the star parallax.

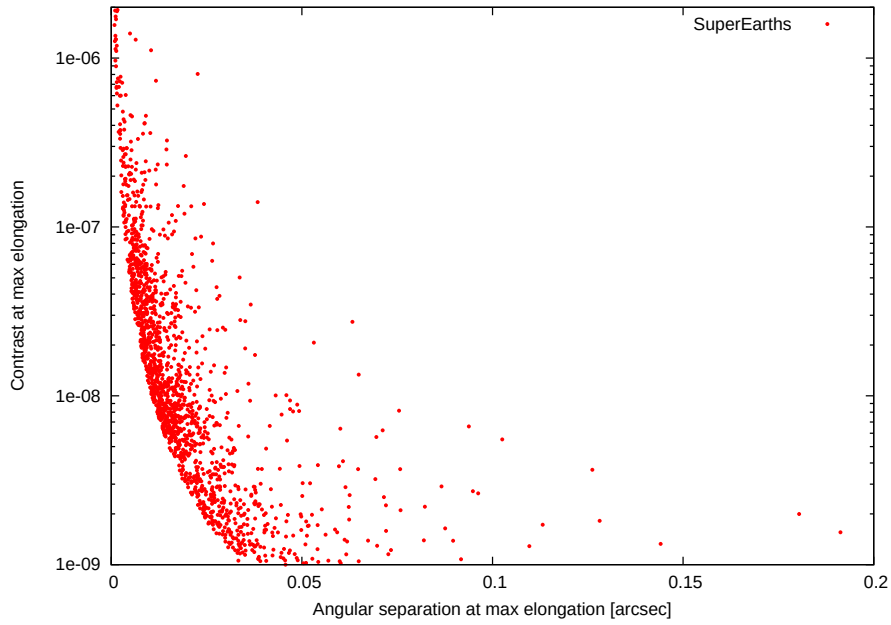

Fig. 1. Angular separation vs reflected light contrast for SuperEarths (2x Earth diameter), assuming each star in the sample has such a planet.

2.3 Apparent magnitudes in visible and near-IR bands

This study assumes that planet imaging is performed in the near-IR with adaptive optics using visible light for wavefront sensing. To estimate the contribution of photon noise, the visible brightness of stars and the near-IR brightnesses of both the stars and their planets are required

The apparent magnitude in the visible bands (V, R and I) are required to estimate how well an adaptive optics system can correct and calibrate the wavefront. These fluxes are therefore important

to derive the detection contrast as a function of angular separation, and are derived using analytical relationships between B-V, V-R, and V-I colors.

Apparent J, H and K magnitudes for the stars are extracted from the 2MASS catalog. In the few cases (1% of the targets) where Gliese catalog entries do not have a match in the 2MASS catalog (usually because they are too faint or they are close companions), 4th order polynomial fits of the V-J, V-H and V-K colors as a function of B-V color are derived from the list of targets that are matched in both catalogs, and then applied to those for which no near-IR flux measurement exists. In this case, the standard deviation in the J, H, and K magnitudes are 0.36, 0.41 and 0.36 respectively (these values are sufficiently small to not significantly affect planet detectability estimates).

Since the planet albedo is assumed independent of wavelength, the planet to star contrast in the near-IR is the same as computed for visible light. No thermal emission is assumed (this is a conservative assumption in K band).

3 Observability of rocky planets in reflected light

3.1 First cut at observation constraints for ELTs

Detectability of exoplanets with direct imaging is a driven by several effects, which are considered in this section to identify if habitable planets can be imaged and characterized with ELTs:

- Angular separation. The separation must be sufficiently larger than the inner working angle (IWA) of the coronagraph.
- Contrast. The planet-to-star contrast must be above the detection limit, which is itself a function of both wavefront correction performance, coronagraph performance, PSF calibration accuracy, and uncorrelated noises (photon noise mostly).
- Star brightness. The star brightness has a strong impact on the wavefront correction quality: faint stars do not produce sufficient light for accurate and fast wavefront measurements.
- Planet brightness. The planet brightness must be above the photon-noise detection limit.

These detectability constraints are highly coupled. For example, the contrast limit is usually a steep function of the angular separation, and both the star brightness and planet brightness strongly affect the contrast limit. The interdependencies between these limits are function of the instrument design and choices (wavefront control techniques, observation wavelength). To easily identify how instrumental trades affect detectability of habitable exoplanets, first cut limits are first applied to construct a small list of potential targets.

Table 1. First cut limits

	limit	comments
Angular separation	$> 1\ \lambda$/D	11mas on a 30-m telescope in H band.
Contrast	> 1e-8	High contrast imaging limit
Planet Brightness	$m_H < 26.8$	Faint detection limit

The first cut limits are shown in table 1. The number of targets kept is mostly driven by the contrast and separation limits, and to a lesser extent by the planet brightness limit. The planet brightness limit is derived from a required SNR=10 detection in 10mn exposure in a 0.05 μm wide effective bandwidth (equivalent to a 15% efficiency for the whole H-band) on a 30-m diffraction limited telescope, taking into account only sky background and assuming all flux in a 20mas wide box is summed. The assumed sky background (continuum + emission) is $m_H = 14.4 mag/arcsec^2$.

The target list after applying the first cut limit consists of 274 entries. This lists consists mostly of relatively faint ($m_V \approx 10$) late-type (V-R $\approx$ 1 to 1.5) main sequence stars. Two notable exceptions are the 40 Eri B and Sirius B white dwarfs, which are much bluer (V-R $\approx$ 0) than the rest of the sample.

3.2 List of most favorable targets

The most favorable target, listed in the table below, were selected with the following criteria:

- Angular separation at maximum elongation > 15 mas
- Contrast > 1e-7
- Planet brightness $m_H < 24$, allowing spectroscopy

The list is composed entirely of nearby late type main sequence stars (spectral types M3.5 to M6). While the contrast level and planet apparent luminosity are quite accessible with an ELT, the angular separation is below 40mas for all targets: none of these hypothetical exoplanets could be directly imaged with the current generation of 8-m to 10-m telescopes.

Table 2. Most favorable targets

Name	Type	Dist.	L_{bol}	m_V	m_R	m_H	Separation	Contrast	$m_H(pl)$
Proxima Centauri	M5.5	1.30 pc	8.64e-04	11.00	9.56	4.83	22.69 mas	8.05e-07	20.07
Barnard's Star	M5	1.83 pc	4.96e-03	9.50	8.18	4.83	38.41 mas	1.40e-07	21.97
Kruger 60 B	M6	3.97 pc	5.81e-03	11.30	9.90	5.04	19.20 mas	1.20e-07	22.35
Ross 154	M4.5	2.93 pc	5.09e-03	10.40	9.11	5.66	24.34 mas	1.37e-07	22.82
Ross 128	M4.5	3.32 pc	3.98e-03	11.10	9.77	5.95	18.99 mas	1.75e-07	22.84
Ross 614 A	M4.5	4.13 pc	5.23e-03	11.10	9.82	5.75	17.51 mas	1.33e-07	22.95
Gl682	M3.5	4.73 pc	6.41e-03	10.90	9.70	5.92	16.93 mas	1.09e-07	23.33
Groombridge 34 B	M6	3.45 pc	5.25e-03	11.00	9.61	6.19	20.98 mas	1.33e-07	23.39
40 Eri C	M4.5	4.83 pc	5.92e-03	11.10	9.88	6.28	15.93 mas	1.18e-07	23.61
Gl 3379	M4	5.37 pc	6.56e-03	11.30	10.06	6.31	15.09 mas	1.06e-07	23.75

Three of the targets are part of close multiple systems: Ross 614B is 3.8AU from target Ross 614A; target Groombridge 34 B is 150AU from its M2 primary; and target 40 Eri C is 35AU from 40 Eri B (white dwarf), 420 AU from 40 Eri A (K1).

4 High efficiency conronagraphy at small IWA on segmented apertures

Phase-induced Amplitude Apodization (PIAA) uses aspheric mirrors to achieve a lossless beam apodization [5], and can therefore produce a highly apodized beam suitable for high contrast imaging without the angular resolution loss and throughput loss of a conventional apodizer. PIAA can also be used to replace the entrance apodization in a Lyot-type coronagraph using a phase-shifting focal plane mask. The resulting coronagraph, denoted Phase-induced Amplitude Apodization Complex mask coronagraph (PIAACMC), offers simultaneously full throughput, sub-λ/D inner working angle and total on-axis extinction [6], and is compatible with segmented ELT pupils.

An example PIAACMC design is shown in figure 2 for a segmented centrally obscured pupil. The entrance pupil P (image shown in the lower left of the figure) is apodized with lossless aspheric PIAA optics. Because the PIAA optics perform apodization by remapping instead of selective transmission, the resulting pupil P1 shape is modified. A conventional apodizing mask may be used to fine-tune the apodization if the PIAA optics do not exactly produce the required amplitude distribution. The resulting pupil A is shown in the second image from the lower left corner. The image of an on-axis point source is shown in the center image, where the phase-shifting partially transmissive focal plane mask is inserted. In the output pupil plane C, all light within the pupil has been removed, while diffracted starlight fills the gap and obstructions of the segmented pupil. A Lyot mask (noted Lmask) can then select only the geometric pupil area (after remapping) to fully block on-axis starlight while fully transmitting the light from distant off-axis source. A well-documented side-effect of apodization with PIAA optics is that off-axis PSFs are highly distorted, and corrective optics (inverse PIAA) are required at the output of the coronagraph to maintain diffraction limited sharp PSFs over a scientifically useful field of view [7].

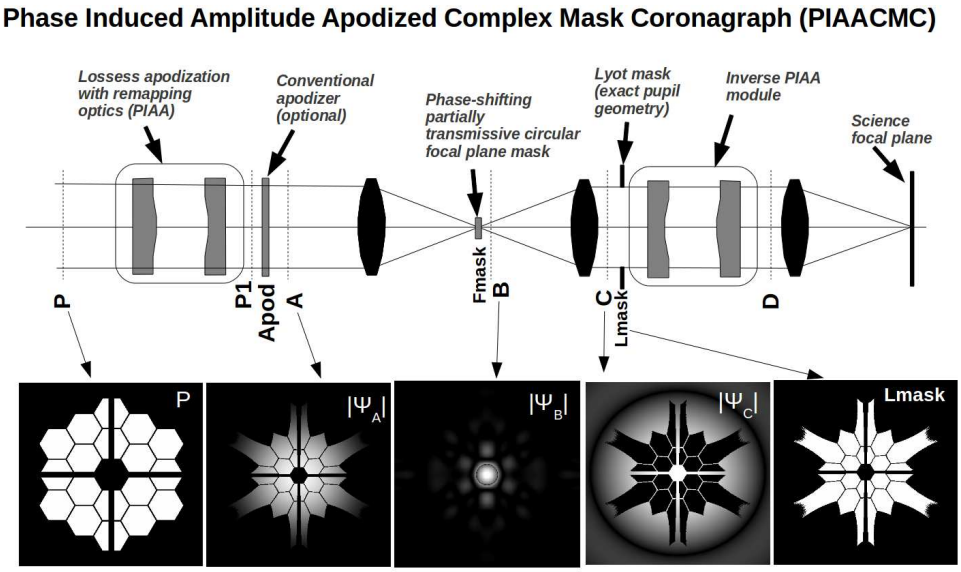

Fig. 2. PIAACMC design for a centrally obscured segmented aperture. The entrance aperture (P) is apodized (P1) thanks to aspheric PIAA optics. The central part of the corresponding on-axis PSF is both attenuated and phase-shifted (B) by the focal plane mask, yielding perfect destructive interference within the geometric pupil (C). The Lyot mask (Lmask) rejects all light from the on-axis source, while it transmits all of the light from distant off-axis sources. Inverse PIAA optics can be introduced to recover a sharp off-axis image over a wide field of view.

5 Wavefront control for high contrast imaging near the telescope's diffraction limit

5.1 Optimal wavefront sensing strategy

The photon-noise wavefront sensing precision for a given exposure time is proportional to $\sqrt{Nph}/\lambda_{WFS}$. The relative sensitivity between two colors λ_1 and λ_2, in the photon noise limited regime for a constant relative spectral bandwidth, is:

$$S(\lambda_1, \lambda_2) = \frac{\lambda_2 \sqrt{zp_1}}{\lambda_1 \sqrt{zp_2}} \, 2.51188643^{(m_2 - m_1)/2} \tag{2}$$

Where zp_1 and zp_2 are the magnitude scale zero points at λ_1 and λ_2. m_1 and m_2 are the magnitudes at λ_1 and λ_2. The $S(\lambda_1, \lambda_2)$ is greater than 1 if wavefront sensing is more precise at λ_1 than at λ_2. Since the typical targets have $V - R = 1.3$, $V - I = 3.0$ and $V - H = 5.0$ colors, equation 2 gives:

$$S(V,R) = 0.76 \; ; \; S(V,I) = 0.546 \; ; \; S(V,H) = 0.97 \tag{3}$$

The targets are therefore sufficiently red for I-band to be significantly better for wavefront sensing than V band, and the performance in R band wavefront sensing is intermediate. The photon-noise limited wavefront measurement error in I band is close to being half what it would be if V band was used. In addition to this photon-noise advantage, I-band wavefront sensing minimizes chromatic non-common path errors with the near-IR scientific imaging wavelength, while allowing non-overlapping spectral bands between wavefront sensing and scientific imaging. Interestingly, even if low-noise fast detectors were available in the near-IR, it is not as good for wavefront sensing as I-band, as the increased number of photon in the near-IR is not sufficient to compensate the longer wavelength. It is thus assumed in this study that wavefront sensing is performed in I-band, where low noise high quantum efficiency fast detectors exist.

5.2 Expected raw and detection constrast limits

The raw PSF contrast is estimated in figure 3 for a $m_I = 8.5$ target representative of a faint target in our sample using an analytical model [8]. In the 10 to 20 mas angular separation range where most of the exoplanets are imaged, the contrast is limited by time lag in the loop and photon noise, and the other fundamental limits to raw contrast (scintillation and atmospheric chromaticity effects) are much smaller. With a high efficiency wavefront sensor able to take advantage of the telescope's diffraction limit, the expected raw PSF contrast at these small separations is approximately 1e-5, provided that the servo lag is no more than about 0.1 ms. This unusually low servo lag can be achieved with a high WFS sampling frequency (>10 kHz), and/or the use of predictive wavefront control techniques. Figure x also shows that a seeing-limited WFS such as the SHWFS is very inefficient at these small angular separations, and would be a poor choice for the system, even if it operates at its photon-noise limit with no loop servo lag other than the one imposed by photon noise.

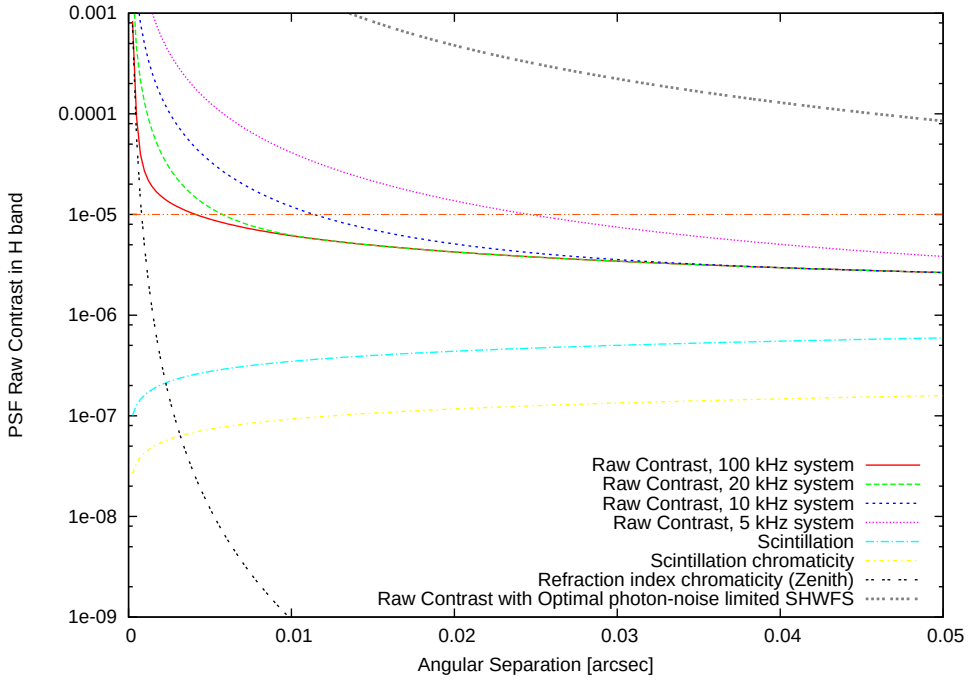

Fig. 3. Raw contrast in a Extreme-AO corrected PSF on a 30-m telescope. The WFS is assumed to be operating at the diffraction limited sensitivity on a $m_I = 8.5$ target, with a 0.05 μm effective spectral bandwidth. For comparison, the photon-noise limited raw contrast limit for a SHWFS is also shown (upper curve). Several closed loop effective delays have been considered.

The analytical model used to estimate raw contrast was also tested for an 8-m diameter telescope under the same conditions. For a 1 kHz system with a diffraction-limited wavefront sensor on an 8-m telescope, the raw contrast at 0.1" is 3e-4 (limited by servo lag), and it is 3e-5 at 0.5". These numbers are consistent with the goals of the future Extreme-AO systems on such telescopes.

The detection contrast limit is more difficult to estimate for this system, as a range of PSF calibration techniques could be used (spectral or polarimetric differentiation for example). For simplicity, it is assumed here that spectral or polarimetric PSF calibration techniques are not used, and that the detection limit is imposed by speckle structure in the long-exposure image and photon noise. It is also assumed that static and slow speckles that are not due to the atmosphere are removed by focal plane wavefront control, a scheme that has already demonstrate control and removal of static coherent speckles at the 3e-9 contrast level in the presence of much stronger dynamic speckles [9].

The PSF halo consists of rapid atmospheric speckles at the 1e-5 contrast level with a lifetime of no more than one millisecond (speckles of longer duration are suppressed by the AO loop). In a one-hour observation, this fast component can thus average to 5e-9 contrast assuming that the AO system has removed correlation on timescales above 1ms. In addition to these fast speckles, chromatic non-common path errors and scintillation create a speckle halo contribution at the 1e-6 contrast level. Since this component is not controlled by the AO system, its coherence time is longer, at up to about 100ms in the near-IR. A 1-hr long observation will average this component by a factor ≈200, to 5e-9 contrast level. Finally, photon noise in a 1-hr exposure for a $m_H = 6$ star and a 1e-5 raw contrast will set a 1e-9 contrast limit for a 0.05 μm effective spectral bandwidth. Combined together, the 3 effects lead to a detection contrast limit just below 1e-8 for a 1hr long exposure.

6 Instrument Design, technologies required

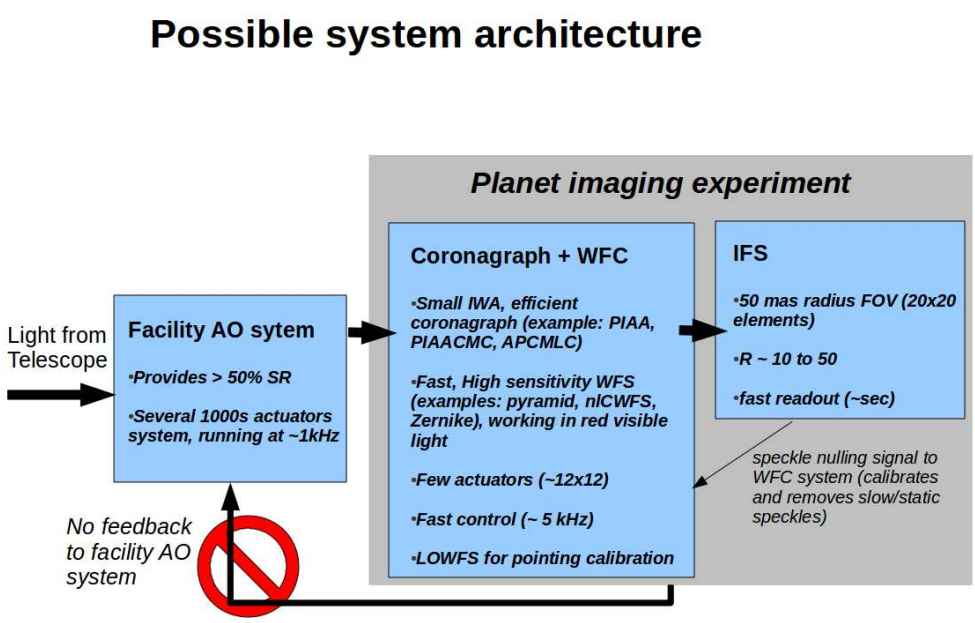

Fig. 4. Possible system architecture for an experiment aimed at imaging habitable planets around nearby M-type stars with an ELT.

A possible system architecture is shown in figure 4, and designed to be as simple as possible while meeting the requirements listed in this paper. Its main characteristics are:

- Given that the ExAO system needs to operate fast (10 kHz or faster) but does not need to clean the PSF halo over a large range of angles, it consists of a ultra fast low actuator count system (≈12 x 12 actuators) placed after a conventional facility AO system. The conventional AO system's role is to provide a diffraction-limited PSF, and will require many actuators for an ELT, but can run relatively slowly (kHz). The ExAO system achieves its speed and sensitivity over a small number of modes to keep its computational bandwidth and pixel read rate manageable. This architecture (slow tweeter followed by fast woofer) is opposite to current ExAO systems for which the second AO layer has a higher actuator count.
- Since the two AO systems have different functions and very different temporal bandwidth, there is no need for communication between the two systems. The planet imaging instrument does therefore not need to interface with the facility AO system, simplifying development, testing and operation.

– A fast sensor dedicated to pointing and focus is implemented within the coronagraph [10, 11].
– The coronagraph allows direct imaging at λ/D inner working angle
– The science camera - an integral field spectrograph - is designed for fast readout, compromising with field of view and spectral resolution. The fast readout (second or faster) allows efficient active suppression of slow speckles that are due to non-common path errors in the system.

7 Conclusions

Direct imaging of habitable planets around nearby M-type stars with ELTs appears to be feasible thanks to new techniques that allow high contrast imaging at small angular separation. While these planets are too close to be resolved by current telescopes, an ELT able to acquire high contrast imaging in the 10mas to 30mas separation range can image them, and their relatively high brightness would allow for spectroscopic investigations. For the top targets, Earth-size habitable exoplanet may even be detected.

The technologies required to achieve this goal exist, even though several key technologies have only recently been identified and not yet demonstrated at the required performance level in laboratories or on sky. The next decade will be extremely valuable to mature these techniques toward an integrated system that can be ready when ELTs begin science operations. Experimental systems on 8-m telescopes, such as the Subaru Coronagraphic ExtremeAO (SCExAO) instrument, are rapidly maturing the techniques proposed required for this goal, and should continue to do so through this decade. Given the unusual requirements of such a system and the relatively small number of targets, a focused instrument (more akin to a science experiment than a facility instrument) should be developed instead of a general purpose extreme-AO system similar to the current generation of ExAO systems on 8-m class telescopes. This would allow for a relatively simple system with a rapid development schedule and moderate cost - an approach that would allow ELTs to acquire the first high quality spectra of nearby M-type habitable planets. This science goal is complementary to future space mission operating in visible light, which will need to target exoplanets at more challenging contrast levels around Sun-like stars due to limited angular resolution.

References

1. Gliese, W., Jahreiss, H. *Preliminary Version of the Third Catalogue of Nearby Stars* (NASA/Astronomical Data Center, 1991)
2. M.F. Skrutskie, R.M. Cutri, R. Stiening, M.D. Weinberg, S. Schneider, J.M. Carpenter, C. Beichman, R. Capps, T. Chester, J. Elias, J. Huchra, J. Liebert, C. Lonsdale, D.G. Monet, S. Price, P. Seitzer, T. Jarrett, J.D. Kirkpatrick, J. Gizis, E. Howard, T. Evans, J. Fowler, L. Fullmer, R. Hurt, R. Light, E.L. Kopan, K.A. Marsh, H.L. McCallon, R. Tam, S. Van Dyk, and S. Wheelock, AJ, **131**,(2006),p. 1163.
3. Stauffer, John; Tanner, Angelle M.; Bryden, Geoffrey; Ramirez, Solange; Berriman, Bruce; Ciardi, David R.; Kane, Stephen R.; Mizusawa, Trisha; Payne, Alan; Plavchan, Peter; von Braun, Kaspar; Wyatt, Pamela; Kirkpatrick, J. Davy, PASP, **122**, (2010), p. 885
4. Reid, N.I., Hawley, S.L. & Gizis, J.E. 1995, ApJ **110**, (1995), p.1838
5. Guyon, O., Pluzhnik, E.A., Galicher, R., Martinache, F., Ridgway, S.T., Woodruff, R.A., ApJ, **622**, (2005), p. 744
6. Guyon, O., Martinache, F., Belikov, R., Soummer, R., ApJ, **190**, (2010), p. 220
7. Lozi, J., Martinache, F., Guyon, O., PASP, **121**, (2009) pp. 1232-1244
8. Guyon, O., ApJ, **629**, (2005), p. 592
9. Guyon, O., Pluzhnik, E.A., Martinache, F., Totems, J., Tanaka, S., Matsuo, T., Blain, C., Belikov, R., PASP, **122**, (2010), p. 71
10. Guyon, O., Matsuo, T., Angel, R., ApJ, 693, (2009) pp 75-84
11. Vogt, F.P.A., Martinache, F., Guyon, O., Yoshikawa, T., Yokochi, K., Garrel, V., Matsuo, T., PASP, 123, (2011) p. 1434